

A New General Paradigm for Understanding and Preventing Li Metal Penetration through Solid Electrolytes

Yue Qi¹, Chunmei Ban^{2*}, and Stephen J. Harris³

¹ School of Engineering, Brown University, Providence, RI, 02912, USA

² Mechanical Engineering, University of Colorado Boulder, Boulder, CO, 80309, USA

³ Energy Storage Division, Lawrence Berkeley National Laboratory, Berkeley, CA 94720, USA

Abstract

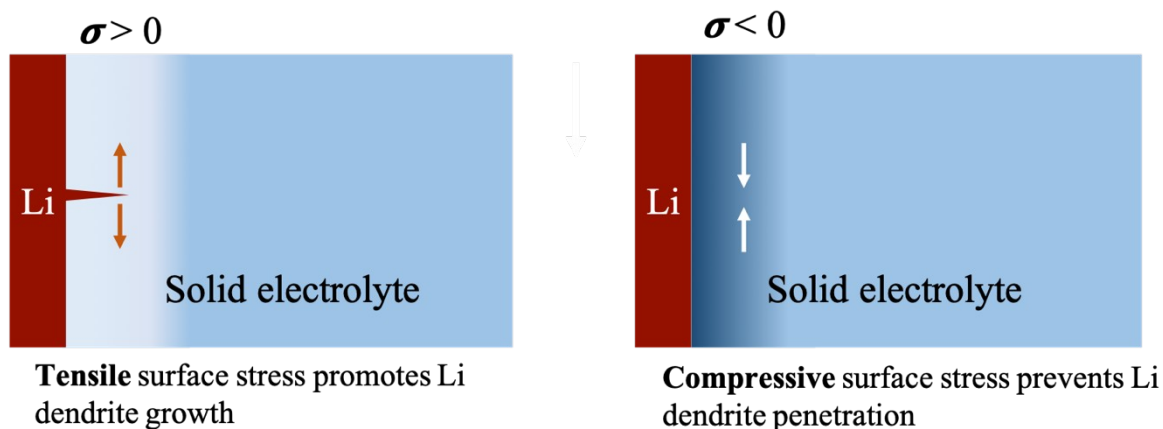
The use of lithium (Li) or sodium (Na) metal anodes together with highly ion-conductive solid electrolytes (SEs) could provide batteries with a step improvement in volumetric and gravimetric energy densities. Unfortunately, these SEs face significant technical challenges, in large part because Li and Na dendrites can penetrate through the SEs, leading to short circuits. The ability of such a soft material (Li or Na metal) to penetrate through a ceramic is surprising from the point of view of models widely used in the Li battery field.

We introduce a concept, new to the battery field, for preventing penetration of lithium dendrites through SEs by putting the SE surfaces into a state of residual compressive stress. For a sufficiently high compressive stress, cracks have difficulty forming, and cracks that do form are forced to close, inhibiting dendrite penetration. This approach is widely used to solve commercially important stress corrosion cracking problems in metals and static fatigue problems in ceramics and glasses (e.g., Gorilla Glass). However, the technique will not be useful for SEs if

* Correspondence: chunmei.ban@colorado.edu

21 the Li ion transport rate through a SE is substantially reduced when the SE is in compression.
22 Our molecular dynamics calculations for Li ion transport through a common SE demonstrate that
23 the introduction of even very high residual compressive stresses (~ 10 GPa) has only a modest
24 effect on Li ion transport kinetics, suggesting that the approach is viable and capable of
25 providing a new paradigm for developing high-performance and mechanically stable SEs.

26 TOC Graphic



27

28 Introduction

29 The use of Li or Na metal negative electrodes (anodes) could provide a substantial increase in the
30 gravimetric and volumetric energy density for Li batteries. However, their use in high capacity
31 rechargeable batteries has been precluded, in large part, because of the growth of Li filaments
32 (loosely called “dendrites”).¹ The filaments provide surfaces for degradation reactions, and they
33 may become electrically isolated. Dendrite penetration into solid electrolytes, which occurs
34 readily,² can induce mechanical failure and fracture of solid electrolytes, and if the dendrites

35 reach the positive electrode, they will cause a short circuit, potentially leading thermal runaway
36 or fire.³⁻⁸

37 The battery community has taken several approaches to addressing the dendrite penetration
38 problem.^{9,10} Monroe and Newman and followers proposed an electrochemical-mechanical
39 model in which Li metal with a small protrusion (proto-dendrite) is pressed conformally, or
40 nearly conformally, against a solid polymer separator.¹¹⁻¹³ They found that a sufficiently high
41 separator shear modulus, could prevent penetration. However, neither suppression of dendrite
42 penetration in liquid electrolyte cells under moderate stack pressures,^{14,15} nor penetration through
43 solid electrolytes with very high shear moduli—cases that do not involve solid polymer
44 separators—can be readily explained with this paradigm.^{2,16} We attribute this discrepancy to a
45 combination of the model not incorporating Li creep; ignoring internal defects in the solid
46 electrolyte; and assuming near-conformal contact, which is not realized for interfaces between Li
47 metal and either thin commercial separators or solid electrolytes under commercially feasible
48 pressures.^{14,16} It is important to note that because only a small fraction of the Li metal and solid
49 electrolyte surfaces are in physical contact¹⁶, GPa-level hydrostatic pressures in Li cannot¹⁷ build
50 up against SEs because Li rapidly relaxes, by deformation and creep, into non-contact regions
51 that may be at a considerable distance from the contact point. Even if contact is conformal inside
52 cracks, Li will still be readily squeezed out of the crack at the dendrite's base if the hydrostatic
53 pressure climbs to or above the Li hardness, given the very high sensitivity of the creep rate to
54 stress.¹⁸ We note that the MPa-level stresses that are possible are too small to affect the plating
55 reaction,¹⁴ while GPa-level compressive stresses could significantly inhibit plating.¹⁷ Thus, we
56 believe that contact mechanics between Li and a solid electrolyte cannot be properly modeled on

57 a scale of a single penetrating dendrite. In addition, internal defects, such as pores, cracks, and
58 grain boundaries in solid electrolytes can trap electrons and nucleate metallic Li, even ahead of
59 the Li-metal front.¹⁹

60 Chemical and physical modifications to the Li-separator interface, such as introduction of
61 nanostructures or coatings or by modification of the electrolyte,²⁰⁻³⁴ have seen some success in
62 inhibiting dendrite growth, while other approaches have focused on developing new solid
63 electrolytes and special Li hosts or on controlling the temperature.^{35,36,37,38} Nevertheless, to date
64 there are no commercially available high capacity rechargeable Li metal batteries that operate at
65 current densities comparable to those in liquid electrolytes, in significant part because of the
66 dendrite penetration problem. This Perspective proposes a new paradigm for eliminating
67 dendrite-induced short circuits.

68 **A New Approach to Suppress Lithium-Dendrite Penetration of SEs**

69 Our proposed approach is based on an analogy to stress corrosion cracking (SCC),³⁹⁻⁴² which has
70 been studied and largely solved in the corrosion field. SCC occurs when the surface of a
71 component is chemically (usually electrochemically) attacked at a defect or heterogeneity.⁴³ The
72 result is the formation or extension of an incipient crack that can grow if and only if the crack tip
73 is in a sufficiently high state of tension. Thus, SCC crack growth occurs under the combined
74 effect of a chemical reaction plus local tensile stresses that are above some threshold value but
75 below the level required for fast crack propagation.^{44,45} SCC has led to catastrophic results, such
76 as the collapse of the Silver Bridge across the Ohio River. In that case, local rusting led to stress
77 corrosion cracks that followed grain boundaries in the steel.^{46,47} Although SCC is often thought of

78 as occurring primarily in metals, it can also occur in glasses, ceramics, and quartz, where the
79 process is known as static fatigue.⁴⁸⁻⁵³

80 Since the attacking medium in SCC is usually water, shear strength^{11,12} plays no role, so the fact
81 that soft Li metal penetrates through hard ceramic solid electrolytes is not surprising if SCC is
82 the mechanism.^{11,12} Furthermore, high

83 hydrostatic pressures in the Li are not required,
84 since the SCC driving force comes from chemical
85 reactions in regions of tensile stress in the solid
86 electrolyte rather than from pressure. The
87 proposed analogy between water penetration and
88 Li metal penetration is visualized in **Figure 1**,

89 which shows stainless steel that has been attacked
90 by water via SCC,⁵⁴ where intergranular cracks
91 were observed during aging at 550 °C, **Figure**
92 **1(a)**. The formation of chromium carbides along
93 the grain boundaries, which is facile at elevated

94 temperature, results in creation of a chromium-depleted region, exacerbating the susceptibility to
95 intergranular corrosion when tensile stresses are present. **Figure 1c** shows intergranular

96 penetration of LLZO by Li metal, forming dendrites as the cracks propagate.² As illustrated in
97 **Figures 1b** and **1d**, both processes involve corrosive/electrochemical environments together with

98 the presence of heterogeneities,⁴³ including grain boundaries, contaminants, or precipitates. We
99 suggest that, in analogy with SCC, local residual tensile stresses promote Li dendrite penetration

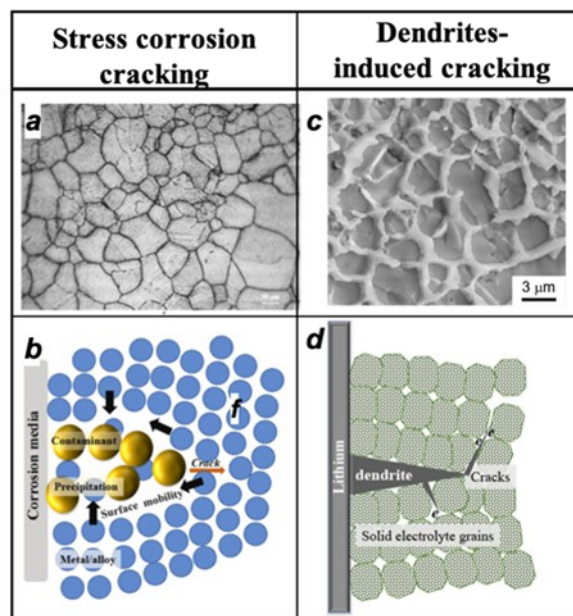


Figure 1: SEM images of (a) intergranular cracking in stainless steel (b) the intergranular penetration of LLZO by Li. Schematic of (c) SCC propagation and (d) lithium penetration into LLZO.

100 via crack propagation. Detailed modeling demonstrates how tensile stresses and crack
101 propagation interact in secondary NMC particles.⁵⁵

102 An approach that often solves SCC problems is putting the surface into a state of residual
103 compressive stress. For example, the crack resistance of Gorilla Glass is due to exchanging
104 smaller sodium atoms near the surface with larger potassium atoms.⁵⁶

105 We are not aware of any spatially resolved surface stress measurements in solid electrolytes,
106 although residual tensile stresses above 100 MPa in LLZT were observed from SPS processing.⁵⁷
107 Experiment shows that when tensile, such stresses can result in highly brittle products.⁵⁸ Local
108 tensile residual stresses can also be generated from heterogeneities as well as from machining or
109 polishing.⁵⁹⁻⁶² Thus, solid electrolytes may be readily susceptible to an analog of SCC (or static
110 fatigue) as well as to brittle fracture.

111 However, the analogy between solving SCC and solving Li dendrite penetration is imperfect
112 because a solid electrolyte must also maintain sufficient ionic conductivity after the compression
113 is introduced, a factor that is irrelevant for something like Gorilla Glass. Previous work has
114 shown that internal stresses can have a significant impact on ionic conductivity, and it is possible
115 that putting the solid electrolyte into compression could substantially hinder ion mobility.⁶³⁻⁶⁹

116 **Evaluation of the Impact of Stress on Li Diffusion**

117 To evaluate the effect of a hydrostatic compressive stress on Li diffusion kinetics, molecular
118 dynamics (MD) simulations were performed as described in the Methods section. Results are
119 shown in **Figure 2(a)**, which were calculated at 1100K to accelerate the diffusion process. The

120 Li self-diffusivity D
 121 in LLZO was fitted
 122 to the linear region
 123 of the root mean
 124 square distance
 125 (RMSD) vs
 126 simulation time.
 127 The diffusivity was
 128 then plotted as a
 129 function of the average hydrostatic pressure.

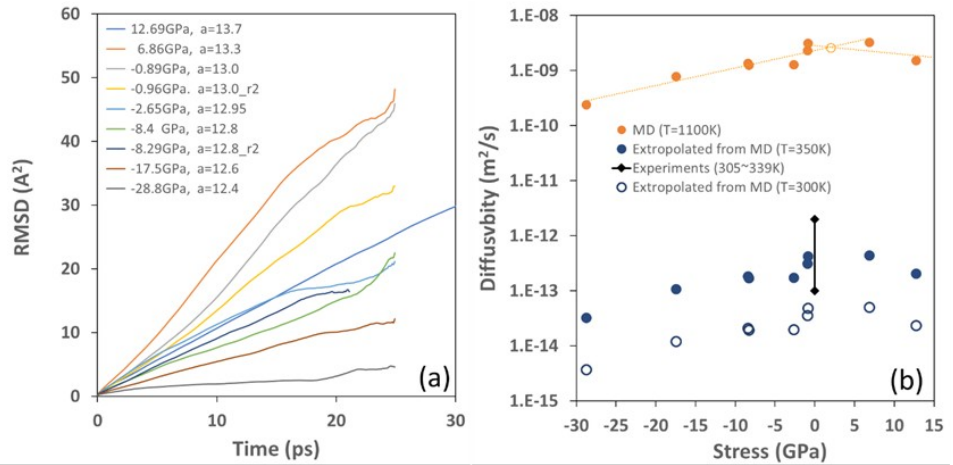


Figure 2. (a) Simulated average Li RMSD vs. simulation time with varying lattice parameters. (b) Li self-diffusivity as a function of stress (positive stress means tension). The dotted lines fitting the diffusivity with positive and negative slopes intersect at 2 GPa and a peak stress of $2.6 \times 10^{-9} \text{ m}^2/\text{s}$.

130 Simulation results at 1100K (orange dots, **Figure 2(b)**) show a peak diffusivity of 2 GPa tensile
 131 stress. In order to compare to experiments at room temperature, the simulated diffusivity was
 132 extrapolated to 300K (blue circles) and 350k (blue dots) based on the experimentally measured
 133 activation energy of 0.38 eV, a value that is insensitive to strain, according to density functional
 134 theory (DFT) calculations.^{70,71} The solid blue dots, **Figure 2(b)**, show that the
 135 simulated/extrapolated room temperature Li diffusivity at zero stress is $\sim 0.5 \times 10^{-13} \text{ m}^2/\text{s}$, which
 136 is within the range of experimental values, $0.1 - 2 \times 10^{-12} \text{ m}^2/\text{s}$ ⁷⁰, supporting the MD simulation
 137 results. It is not surprising to see that Li diffusivity peaks around 2 GPa tensile stress because fast
 138 ionic conductivity in LLZO is enabled by low-barrier concerted ion migrations, which are
 139 triggered by the strong ion-ion Coulomb interactions at unique ion configurations. While
 140 compression shrinks the free volume available for Li ion mobility, high tension may reduce the
 141 Coulomb interactions required for fast ion conductivity.

142 Although the Li diffusivity decreases under compression, even at 10 GPa compression the
143 diffusivity is still 40% of its value at zero stress. This difference is even less than the variation of
144 the experimental data at zero stress. Consistent with our results, we note that the experimentally
145 measured Li ion conductivity in LLZO showed minimal changes under compressive residual
146 stresses between 12.5 MPa and 50 MPa.⁷² This observation can be generalized to other solid
147 electrolyte systems. Famprikis et al.⁷³ recently summarized the activation volume, the change of
148 activation barrier to pressure, for cation conduction in many solid electrolytes. Depending on the
149 diffusion carrier (vacancy or interstitial), the activation volume is either positive or negative. All
150 values ($1.7 \pm 1.4 \text{ cm}^3/\text{mol}$) lead to $0.017 \pm 0.014 \text{ eV}$ activation energy change with a pressure of 1
151 GPa. For the commonly used lithium solid electrolytes, less than 5% impedance and 0.01 eV
152 activation energy change were reported in mechanically strained LiPON;⁷⁴ less than 0.02~0.05
153 eV migration barrier change was reported up to a 4% of strain in $\text{Li}_{10}\text{GeP}_2\text{S}_{12}$ and in
154 LLZO.^{67,71,75,71,76} The only exception and discrepancy reported is that the Li migration barrier in
155 $\text{Li}_{10}\text{GeP}_2\text{S}_{12}$ is much higher under compression than tension.⁷⁵ Therefore, we conclude that
156 even very large compressive stresses will not have a large impact on Li ion diffusion over short
157 distances in most of the solid electrolytes.

158 **Methods for Applying Compressive Stress**

159 As mentioned above, SCC can occur only when the surface is in tension, so a highly successful
160 and widely used strategy for preventing SCC has been to put the component's surface into a state
161 of residual compression. If this residual compressive stress is high enough, cracks are difficult to
162 form or grow, and cracks that exist are forced to close. Among the most widely used techniques
163 to introduce a surface residual compressive stress in metals is shot peening,⁷⁷⁻⁸⁰ which is a cold

164 working process where large numbers of small hard particles (metallic, ceramic, or glass)
165 impinge on the component with sufficient force to deform it plastically and put the surface into
166 compression.^{81,82} For brittle materials such as ceramics and glasses, other techniques have been
167 developed for commercial application. Among them are laser shock peening (LSP), which can
168 yield compressive stresses of up to 500 MPa in aluminum oxide;⁸³ ion implantation;^{84,85} and ion
169 exchange^{49,86} (which is used to make Gorilla Glass).^{49,56,86} The latter techniques can introduce
170 compressive residual stresses as high as 10 GPa in aluminum oxide, although much lower
171 stresses are appropriate for metals, typically half the yield stress.⁸⁵ We next consider each of
172 these approaches, except for shot peening, for use with LLZO.

173 LSP introduces laser plasma-driven shock-waves into a material, typically using a plasma-
174 confining medium (e.g., glass or water) to increase the peak pressure of the shock wave. A
175 sacrificial layer is often used to protect the treated sample from laser ablation. Shukla et al.
176 demonstrated that their LSP-treated α -Al₂O₃ had a biaxial compressive residual stress of several
177 hundred MPa that extended to a depth of up to 1.2 mm from the surface.⁸³

178 Ion exchange has also been used to introduce compressive stresses at the surface, typically by
179 exchanging alkali (or sometimes alkaline-earth) ions in the original glass/glass-ceramic with
180 larger ones from a molten salt bath.⁸⁷ The introduction of large ions near the surface induces a
181 volume increase, generating a compressive stress in the ion-exchange region. The final
182 mechanical properties are dependent on the stress level at the surface and the depth of
183 penetration of the larger ions.

184 Unfortunately, the use of these strengthening strategies for preventing Li dendrite penetration
185 through solid electrolytes face potentially severe constraints. In the case of ion exchange, only a
186 limited selection of ions can be introduced. Also, ion exchange strongly favors the exchange of
187 monovalent ions—replacing the Li in this case—whose removal will inhibit Li ion mobility in
188 the exchanged region. While LSP avoids these problems, it may create heterogeneous surface
189 damage that could increase the interface resistance; it can also create local tensile stresses.⁸³
190 Furthermore, the range of stresses introduced by LSP, up to hundreds of MPa, is much lower
191 than what is possible with other techniques.

192 The preferred alternative, in our estimation, is ion implantation, which can be used to introduce
193 residual surface compressive stresses with control of stress level, depth profile, crystallinity, and
194 chemistry in the near-surface region (10 to 1,000 nm). It has been used commercially for decades
195 to strengthen polymers, glasses and ceramics in order to solve stress corrosion cracking (SCC) or
196 static fatigue problems, but it has not been applied to SEs, to our knowledge. An advantage of
197 ion implantation is the large number of chemical, structural, and physical states that can be
198 created, including metastable non-equilibrium states, for nano/mesoscale tailoring the surface
199 structure of SEs.

200 Energetic implanted ions can include transition metal ions, halide ions, rare gas ions, and even
201 lithium ions, which can modify the surface structure—including creating local disorder—leading
202 new mechanical properties for solid
203 electrolytes, as illustrated schematically in

204 **Figure 3.** With its control of dopant species,
205 concentration, and spatial distribution

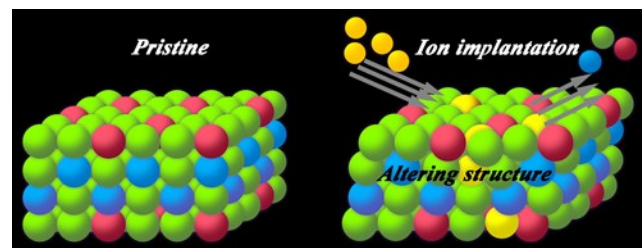


Figure 3: Schematic of using ion implantation to alter structure of solid electrolytes.

206 (implantation depth), ion implantation has also been widely used in modifying electronic
207 properties of semiconductors for the microelectronics industry, as well as strengthening of metals
208 and non-conducting ceramics.⁸⁸ Recent work has shown a positive impact of using ion beam
209 modification on the ionic conductivity of polymer electrolyte films due to increased charge
210 carries and dielectric constant.⁸⁹ Implantation can amorphize the implanted region, but the fact
211 that both crystalline and glassy SEs transport Li ions^{7,58} suggests that this issue may not be
212 severe. Implantation also changes the chemical identity of the implanted region.⁷ Effects of
213 typical implanted doses (less than 1%) on Li ion conductivity will be studied in future work.
214 Minimizing the thickness of the implanted region may ameliorate these issues. Since
215 monovalent ions tend to be mobile, we will concentrate our efforts on polyvalent ions for
216 implantation. Of course, any polishing treatment to remove surface contaminants would have to
217 be performed before implantation.⁹⁰

218 Finally, we note that introduction of compressive residual surface stresses is expected to make
219 any material, including SEs, less brittle and, thus, easier to handle in a commercial environment.
220 We expect that implantation of solid electrolytes will enable materials with properties that can be
221 optimized for batteries as well as for a wide variety of other applications.

222 **Conclusion and Perspective**

223 In summary, inspired by successful work on stress corrosion cracking, we have proposed a new
224 paradigm for inhibiting dendrite penetration through solid electrolytes: we suggest putting the SE
225 surfaces into a state of residual compressive stress in order to inhibit the short circuits—initiating
226 either at the Li surface or from within the SE—that accompany dendrite penetration. We have

227 performed MD simulations to demonstrate that the introduction of even very high (~ 10 GPa)
228 hydrostatic compressive stresses in LLZO has only a modest impact on Li diffusion kinetics,
229 enabling our proposal. In addition to inhibiting dendrite penetration in solid electrolytes,
230 compressive stresses on the order of GPa will improve their fracture toughness and will tend to
231 suppress lithium nucleation in the compressed region inside of solid electrolytes because of an
232 increased overpotential. While there are a number of techniques that can be used commercially
233 to introduce compressive residual stresses, we suggest that ion implantation will be the most
234 useful for this purpose, as it may provide a new avenue for developing controllable, high-
235 performance and stable solid electrolytes.

236 **METHODS**

237 A periodic cubic cell of $\text{Li}_{24}\text{La}_{24}\text{Zr}_{16}\text{O}_{96}$ was simulated using GULP software and implemented in
238 Materials Studio with a force-field including the long-range Coulombic potential, the short-range
239 Buckingham potential, and a core-shell polarizable potential for O atoms following the
240 parameters provided in.⁹¹ The simulation cell length was varied from 12.4 Å to 13.7 Å, and the
241 root mean square displacement (RMSD) of Li^+ ions was tracked during NVT (fixed cell)
242 dynamics.

243 **AUTHOR CONTRIBUTIONS**

244 S.J.H. and C. B. proposed the idea and concepts. Y.Q. did the calculations. All authors
245 contributed equally to the writing of the manuscript.

246 **ACKNOWLEDGEMENTS**

247 S.J.H. gratefully acknowledges valuable discussions with Professor Brian Sheldon of Brown
248 University and Dr. Yuxin Wang of University of Dayton Research. Y.Q. was supported by
249 National Science Foundation through grant number DMR-1832808. S.J.H. was supported by the
250 Assistant Secretary for Energy Efficiency, Vehicle Technologies Office of the U.S. Department
251 of Energy under the Advanced Battery Materials Research Program. C. B acknowledges
252 financial support from the Paul M. Rady Department of Mechanical Engineering at the
253 University of Colorado, Boulder.

254

References: BIBLIOGRAPHY

- 255
256
257 1 Lin, D., Liu, Y. & Cui, Y. Reviving the lithium metal anode for high-energy
258 batteries. *Nature nanotechnology* **12**, 194 (2017).
- 259 2 Cheng, E. J., Sharafi, A. & Sakamoto, J. Intergranular Li metal propagation
260 through polycrystalline Li₆ 25Al₁₀ 25La₃Zr₂O₁₂ ceramic electrolyte.
261 *Electrochimica Acta* **223**, 85-91 (2017).
- 262 3 Cheng, X.-B., Zhang, R., Zhao, C.-Z. & Zhang, Q. Toward safe lithium
263 metal anode in rechargeable batteries: a review. *Chemical reviews* **117**,
264 10403-10473 (2017).
- 265 4 Feng, X. *et al.* Thermal runaway mechanism of lithium ion battery for
266 electric vehicles: A review. *Energy Storage Materials* **10**, 246-267 (2018).
- 267 5 Bieker, G., Winter, M. & Bieker, P. Electrochemical in situ investigations of
268 SEI and dendrite formation on the lithium metal anode. *Physical Chemistry
269 Chemical Physics* **17**, 8670-8679 (2015).
- 270 6 Harris, S. J., Timmons, A. & Pitz, W. J. A combustion chemistry analysis of
271 carbonate solvents used in Li-ion batteries. *Journal of Power Sources* **193**,
272 855-858 (2009).
- 273 7 Porz, L. *et al.* Mechanism of lithium metal penetration through inorganic
274 solid electrolytes. *Advanced Energy Materials* **7**, 1701003 (2017).
- 275 8 Chen, R. *et al.* The Thermal Stability of Lithium Solid Electrolytes with
276 Metallic Lithium. *Joule* **4**, 812-821 (2020).
- 277 9 Tikekar, M. D., Choudhury, S., Tu, Z. & Archer, L. A. Design principles for
278 electrolytes and interfaces for stable lithium-metal batteries. *Nature Energy*
279 **1**, 16114 (2016).

- 280 10 Wu, B. *et al.* The role of the solid electrolyte interphase layer in preventing
281 Li dendrite growth in solid-state batteries. *Energy & Environmental Science*
282 **11**, 1803-1810 (2018).
- 283 11 Monroe, C. & Newman, J. Dendrite growth in lithium/polymer systems a
284 propagation model for liquid electrolytes under galvanostatic conditions.
285 *Journal of The Electrochemical Society* **150**, A1377-A1384 (2003).
- 286 12 Monroe, C. & Newman, J. The effect of interfacial deformation on
287 electrodeposition kinetics. *Journal of The Electrochemical Society* **151**,
288 A880-A886 (2004).
- 289 13 Barai, P., Higa, K. & Srinivasan, V. Effect of initial state of lithium on the
290 propensity for dendrite formation: a theoretical study. *Journal of The*
291 *Electrochemical Society* **164**, A180-A189 (2017).
- 292 14 Zhang, X. *et al.* Rethinking How External Pressure Can Suppress Dendrites
293 in Lithium Metal Batteries. *Journal of The Electrochemical Society* **166**,
294 A3639-A3652 (2019).
- 295 15 Louli, A. J. *et al.* Exploring the Impact of Mechanical Pressure on the
296 Performance of Anode-Free Lithium Metal Cells. *Journal of The*
297 *Electrochemical Society* **166**, A1291-A1299, doi:10.1149/2.0091908jes
298 (2019).
- 299 16 Zhang, X., Wang, Q. J., Harrison, K. L., Roberts, S. A. & Harris, S. J.
300 Pressure-Driven Interface Evolution in Solid-State Lithium Metal Batteries.
301 *Cell Reports Physical Science* **1**, 100012 (2020).
- 302 17 Klinsmann, M., Hildebrand, F. E., Ganser, M. & McMeeking, R. M.
303 Dendritic cracking in solid electrolytes driven by lithium insertion. *Journal*
304 *of Power Sources* **442**, 227226 (2019).

- 305 18 LePage, W. S. *et al.* Lithium Mechanics: Roles of Strain Rate and
306 Temperature and Implications for Lithium Metal Batteries. *Journal of The*
307 *Electrochemical Society* **166**, A89-A97 (2019).
- 308 19 Tian, H.-K., Liu, Z., Ji, Y., Chen, L.-Q. & Qi, Y. Interfacial Electronic
309 Properties Dictate Li Dendrite Growth in Solid Electrolytes. *Chemistry of*
310 *Materials* **31**, 7351-7359 (2019).
- 311 20 Cheng, X. B. *et al.* Dendrite-free lithium deposition induced by uniformly
312 distributed lithium ions for efficient lithium metal batteries. *Advanced*
313 *Materials* **28**, 2888-2895 (2016).
- 314 21 Zhang, R. *et al.* Conductive nanostructured scaffolds render low local
315 current density to inhibit lithium dendrite growth. *Advanced Materials* **28**,
316 2155-2162 (2016).
- 317 22 Li, W. *et al.* The synergetic effect of lithium polysulfide and lithium nitrate
318 to prevent lithium dendrite growth. *Nature communications* **6**, 7436 (2015).
- 319 23 Liu, Y. *et al.* Lithium-coated polymeric matrix as a minimum volume-
320 change and dendrite-free lithium metal anode. *Nature communications* **7**,
321 10992 (2016).
- 322 24 Khurana, R., Schaefer, J. L., Archer, L. A. & Coates, G. W. Suppression of
323 lithium dendrite growth using cross-linked polyethylene/poly (ethylene
324 oxide) electrolytes: a new approach for practical lithium-metal polymer
325 batteries. *Journal of the American Chemical Society* **136**, 7395-7402 (2014).
- 326 25 Ding, F. *et al.* Dendrite-free lithium deposition via self-healing electrostatic
327 shield mechanism. *Journal of the American Chemical Society* **135**, 4450-
328 4456 (2013).

- 329 26 Ren, Y., Shen, Y., Lin, Y. & Nan, C.-W. Direct observation of lithium
330 dendrites inside garnet-type lithium-ion solid electrolyte. *Electrochemistry*
331 *Communications* **57**, 27-30, doi:10.1016/j.elecom.2015.05.001 (2015).
- 332 27 Zhang, Y. *et al.* Dendrite-free lithium deposition with self-aligned nanorod
333 structure. *Nano letters* **14**, 6889-6896 (2014).
- 334 28 Zhou, W. *et al.* Plating a dendrite-free lithium anode with a
335 polymer/ceramic/polymer sandwich electrolyte. *Journal of the American*
336 *Chemical Society* **138**, 9385-9388 (2016).
- 337 29 Brousse, T., Retoux, R., Herterich, U. & Schleich, D. Thin-film crystalline
338 SnO₂-lithium electrodes. *Journal of The Electrochemical Society* **145**, 1-4
339 (1998).
- 340 30 Dudney, N. J. Addition of a thin-film inorganic solid electrolyte (Lipon) as a
341 protective film in lithium batteries with a liquid electrolyte. *Journal of power*
342 *sources* **89**, 176-179 (2000).
- 343 31 Yang, C.-P., Yin, Y.-X., Zhang, S.-F., Li, N.-W. & Guo, Y.-G.
344 Accommodating lithium into 3D current collectors with a submicron
345 skeleton towards long-life lithium metal anodes. *Nature communications* **6**,
346 8058 (2015).
- 347 32 Lin, D. *et al.* Layered reduced graphene oxide with nanoscale interlayer gaps
348 as a stable host for lithium metal anodes. *Nature nanotechnology* **11**, 626
349 (2016).
- 350 33 Kozen, A. C. *et al.* Next-generation lithium metal anode engineering via
351 atomic layer deposition. *ACS nano* **9**, 5884-5892 (2015).

- 352 34 Zeng, S. *et al.* Robust interface layers with redox shuttle reactions suppress
353 the dendrite growth for stable solid-state Li metal batteries. *Journal of*
354 *Energy Chemistry* (2020).
- 355 35 Zhao, C.-Z. *et al.* An anion-immobilized composite electrolyte for dendrite-
356 free lithium metal anodes. *Proceedings of the National Academy of Sciences*
357 **114**, 11069-11074 (2017).
- 358 36 Chi, S. S., Liu, Y., Song, W. L., Fan, L. Z. & Zhang, Q. Prestoring lithium
359 into stable 3D nickel foam host as dendrite-free lithium metal anode.
360 *Advanced Functional Materials* **27**, 1700348 (2017).
- 361 37 Zheng, G. *et al.* Interconnected hollow carbon nanospheres for stable lithium
362 metal anodes. *Nature nanotechnology* **9**, 618 (2014).
- 363 38 Ishikawa, M., Kanemoto, M. & Morita, M. Control of lithium metal anode
364 cycleability by electrolyte temperature. *Journal of power sources* **81**, 217-
365 220 (1999).
- 366 39 Eliaz, N., Shachar, A., Tal, B. & Eliezer, D. Characteristics of hydrogen
367 embrittlement, stress corrosion cracking and tempered martensite
368 embrittlement in high-strength steels. *Engineering Failure Analysis* **9**, 167-
369 184 (2002).
- 370 40 Raja, V. & Shoji, T. *Stress corrosion cracking: theory and practice.*
371 (Elsevier, 2011).
- 372 41 Zeng, R.-c. *et al.* Review of studies on corrosion of magnesium alloys.
373 *Transactions of Nonferrous Metals Society of China* **16**, s763-s771 (2006).
- 374 42 Anderson, O. L. & Grew, P. C. Stress corrosion theory of crack propagation
375 with applications to geophysics. *Reviews of Geophysics* **15**, 77-104 (1977).

- 376 43 Harris, S. J. & Lu, P. Effects of Inhomogeneities—Nanoscale to Mesoscale
377 —on the Durability of Li-Ion Batteries. *The Journal of Physical Chemistry*
378 *C* **117**, 6481-6492, doi:10.1021/jp311431z (2013).
- 379 44 Pereira, H. B., Panossian, Z., Baptista, I. P. & Azevedo, C. R. d. F.
380 Investigation of stress corrosion cracking of austenitic, duplex and super
381 duplex stainless steels under drop evaporation test using synthetic seawater.
382 *Materials Research* **22** (2019).
- 383 45 Rao, A. U., Vasu, V., Govindaraju, M. & Srinadh, K. S. Stress corrosion
384 cracking behaviour of 7xxx aluminum alloys: a literature review.
385 *Transactions of Nonferrous Metals Society of China* **26**, 1447-1471 (2016).
- 386 46 Lichtenstein, A. G. The silver bridge collapse recounted. *Journal of*
387 *performance of constructed facilities* **7**, 249-261 (1993).
- 388 47 *Silver Bridge*, <https://en.wikipedia.org/wiki/Silver_Bridge> (
389 48 Wiederhorn, S. & Bolz, L. Stress corrosion and static fatigue of glass.
390 *Journal of the American Ceramic Society* **53**, 543-548 (1970).
- 391 49 Gy, R. Stress corrosion of silicate glass: a review. *Journal of non-crystalline*
392 *solids* **316**, 1-11 (2003).
- 393 50 Lade, P. V. & Karimpour, H. Static fatigue controls particle crushing and
394 time effects in granular materials. *Soils and foundations* **50**, 573-583 (2010).
- 395 51 Purnell, P. & Beddows, J. Durability and simulated ageing of new matrix
396 glass fibre reinforced concrete. *Cement and Concrete Composites* **27**, 875-
397 884 (2005).
- 398 52 Teoh, S. Fatigue of biomaterials: a review. *International journal of fatigue*
399 **22**, 825-837 (2000).

400 53 Seaman, J. H., Blanchet, T. A. & Tomozawa, M. Origin of the static fatigue
401 limit in oxide glasses. *Journal of the American Ceramic Society* **99**, 3600-
402 3609 (2016).

403 54 *Different types of corrosion*, WebCorr Corrosion Consulting Services,
404 <[https://www.corrosionclinic.com/types_of_corrosion/intergranular_corrosi](https://www.corrosionclinic.com/types_of_corrosion/intergranular_corrosion_cracking.htm)
405 [on_cracking.htm](https://www.corrosionclinic.com/types_of_corrosion/intergranular_corrosion_cracking.htm)> (

406 55 Zhao, Y. *et al.* A review on modeling of electro-chemo-mechanics in
407 lithium-ion batteries. *Journal of Power Sources* **413**, 259-283 (2019).

408 56 Li, X., Jiang, L., Zhang, X. & Yan, Y. Influence of residual compressive
409 stress on nanoindentation response of ion-exchanged aluminosilicate float
410 glass on air and tin sides. *Journal of non-crystalline solids* **385**, 1-8 (2014).

411 57 Yamada, H. in *Solid Electrolytes for Advanced Applications* 91-110
412 (Springer, 2019).

413 58 Garcia-Mendez, R., Smith, J. G., Neufeind, J. C., Siegel, D. J. & Sakamoto,
414 J. Correlating Macro and Atomic Structure with Elastic Properties and Ionic
415 Transport of Glassy Li₂S-P₂S₅ (LPS) Solid Electrolyte for Solid-State Li
416 Metal Batteries. *Advanced Energy Materials* (2020).

417 59 Trail, S. & Bowen, P. Effects of stress concentrations on the fatigue life of a
418 gamma-based titanium aluminide. *Materials Science and Engineering: A*
419 **192**, 427-434 (1995).

420 60 Liu, D., Shi, Y., Lin, X. & Xian, C. Study on improving surface residual
421 stress of polished blade after polishing based on two-stage parameter
422 method. *The International Journal of Advanced Manufacturing Technology*
423 **100**, 1491-1503 (2019).

424 61 Marshall, D. & Lawn, B. R. Residual stress effects in sharp contact cracking.
425 *Journal of materials science* **14**, 2001-2012 (1979).

- 426 62 Wu, D., Wang, H., Zhang, K. & Lin, X. Research on flexible adaptive CNC
427 polishing process and residual stress of blisk blade. *The International*
428 *Journal of Advanced Manufacturing Technology* **103**, 2495-2513 (2019).
- 429 63 Pan, J. *et al.* Effects of stress on lithium transport in amorphous silicon
430 electrodes for lithium-ion batteries. *Nano Energy* **13**, 192-199 (2015).
- 431 64 Fluri, A., Pergolesi, D., Roddatis, V., Wokaun, A. & Lippert, T. In situ stress
432 observation in oxide films and how tensile stress influences oxygen ion
433 conduction. *Nature communications* **7**, 10692 (2016).
- 434 65 Bucci, G., Talamini, B., Renuka Balakrishna, A., Chiang, Y.-M. & Carter,
435 W. C. Mechanical instability of electrode-electrolyte interfaces in solid-state
436 batteries. *Physical Review Materials* **2**,
437 doi:10.1103/PhysRevMaterials.2.105407 (2018).
- 438 66 De Souza, R. A., Ramadan, A. & Hörner, S. Modifying the barriers for
439 oxygen-vacancy migration in fluorite-structured CeO₂ electrolytes through
440 strain: a computer simulation study. *Energy & Environmental Science* **5**,
441 5445-5453 (2012).
- 442 67 Chen, B. *et al.* Strain tunable ionic transport properties and electrochemical
443 window of Li₁₀GeP₂S₁₂ superionic conductor. *Computational Materials*
444 *Science* **153**, 170-175 (2018).
- 445 68 Atkinson, A. & Ramos, T. Chemically-induced stresses in ceramic oxygen
446 ion-conducting membranes. *Solid State Ionics* **129**, 259-269 (2000).
- 447 69 Liu, W., Liu, H., Ou, G. & Pan, W. Residual stress-dependent electric
448 conductivity of sputtered co-doped CeO₂ thin-film electrolyte. *Journal of*
449 *Applied Physics* **109**, 084321 (2011).

- 450 70 Hayamizu, K., Terada, Y., Kataoka, K., Akimoto, J. & Haishi, T.
451 Relationship between Li⁺ diffusion and ion conduction for single-crystal and
452 powder garnet-type electrolytes studied by ⁷Li PGSE NMR spectroscopy.
453 *Physical Chemistry Chemical Physics* **21**, 23589-23597 (2019).
- 454 71 Moradabadi, A. & Kaghazchi, P. Effect of lattice and dopant-induced strain
455 on the conductivity of solid electrolytes: application of the elastic dipole
456 method. *Materialia* **9**, 100607 (2020).
- 457 72 Yamada, H., Ito, T., Basappa, R. H., Bekarevich, R. & Mitsuishi, K.
458 Influence of strain on local structure and lithium ionic conduction in garnet-
459 type solid electrolyte. *Journal of Power Sources* **368**, 97-106 (2017).
- 460 73 Famprakis, T. *et al.* Under Pressure: Mechanochemical Effects on Structure
461 and Ion Conduction in the Sodium-Ion Solid Electrolyte Na₃PS₄. (2020).
- 462 74 Glenneberg, J., Bardenhagen, I., Langer, F., Busse, M. & Kun, R. Time
463 resolved impedance spectroscopy analysis of lithium phosphorous
464 oxynitride-LiPON layers under mechanical stress. *Journal of Power Sources*
465 **359**, 157-165 (2017).
- 466 75 Ong, S. P. *et al.* Phase stability, electrochemical stability and ionic
467 conductivity of the Li₁₀Æ1 MP₂X₁₂ (M ¹/₄ Ge, Si, Sn, Al or P, and X ¹/₄ O,
468 S or Se) family of superionic conductors.
- 469 76 Andriyevsky, B., Doll, K. & Jacob, T. Ab initio molecular dynamics study
470 of lithium diffusion in tetragonal Li₇La₃Zr₂O₁₂. *Materials Chemistry and*
471 *Physics* **185**, 210-217 (2017).
- 472 77 Hammond, D. & Meguid, S. Crack propagation in the presence of shot-
473 peening residual stresses. *Engineering Fracture Mechanics* **37**, 373-387
474 (1990).

- 475 78 Kobayashi, M., Matsui, T. & Murakami, Y. Mechanism of creation of
476 compressive residual stress by shot peening. *International journal of fatigue*
477 **20**, 351-357 (1998).
- 478 79 Meguid, S., Shagal, G., Stranart, J. & Daly, J. Three-dimensional dynamic
479 finite element analysis of shot-peening induced residual stresses. *Finite*
480 *elements in analysis and design* **31**, 179-191 (1999).
- 481 80 Wang, S., Li, Y., Yao, M. & Wang, R. Compressive residual stress
482 introduced by shot peening. *Journal of Materials Processing Technology* **73**,
483 64-73 (1998).
- 484 81 Mochizuki, M. Control of welding residual stress for ensuring integrity
485 against fatigue and stress–corrosion cracking. *Nuclear Engineering and*
486 *Design* **237**, 107-123 (2007).
- 487 82 Mahmoudi, A., Ghasemi, A., Farrahi, G. & Sherafatnia, K. A comprehensive
488 experimental and numerical study on redistribution of residual stresses by
489 shot peening. *Materials & Design* **90**, 478-487 (2016).
- 490 83 Shukla, P. P., Swanson, P. T. & Page, C. J. Laser shock peening and
491 mechanical shot peening processes applicable for the surface treatment of
492 technical grade ceramics: a review. *Proceedings of the Institution of*
493 *Mechanical Engineers, Part B: Journal of Engineering Manufacture* **228**,
494 639-652 (2014).
- 495 84 Burnett, P. & Page, T. F. An investigation of ion implantation-induced near-
496 surface stresses and their effects in sapphire and glass. *Journal of materials*
497 *science* **20**, 4624-4646 (1985).

498 85 McHargue, C., O'hern, M., White, C. & Lewis, M. Ion implantation in
499 ceramics-residual stress and properties. *Materials Science and Engineering:*
500 *A* **115**, 361-367 (1989).

501 86 Abouelleil, M. M. Ion exchange in glasses and crystals. *Annual Review of*
502 *Materials Science* **23**, 255-268 (1993).

503 87 Chen, W. W. & Wang, Q. J. Thermomechanical analysis of elastoplastic
504 bodies in a sliding spherical contact and the effects of sliding speed, heat
505 partition, and thermal softening. *Journal of Tribology* **130**, 041402 (2008).

506 88 Conrad, J. R., Radtke, J. L., Dodd, R. A., Worzala, F. J. & Tran, N. C.
507 Plasma source ion-implantation technique for surface modification of
508 materials. *Journal of Applied Physics* **62**, 4591-4596 (1987).

509 89 Singh, D. *et al.* in *Macromolecular symposia*. 8-13 (Wiley Online Library).

510 90 Sharafi, A. *et al.* Surface chemistry mechanism of ultra-low interfacial
511 resistance in the solid-state electrolyte $\text{Li}_7\text{La}_3\text{Zr}_2\text{O}_{12}$. *Chemistry of*
512 *Materials* **29**, 7961-7968 (2017).

513 91 Klenk, M. & Lai, W. Local structure and dynamics of lithium garnet ionic
514 conductors: tetragonal and cubic $\text{Li}_7\text{La}_3\text{Zr}_2\text{O}_7$. *Physical Chemistry*
515 *Chemical Physics* **17**, 8758-8768 (2015).

516

517

518 **Figure Legends**

519 **Figure 1:** Comparison between the intergranular cracks caused by SCC and Li intergranular
520 penetration into LLZO. Surface morphology of SCC propagation and the intergranular
521 penetration of LLZO by Li are shown in (a) and (c), respectively. Reprint with permission from
522 ref. 2 and 54. Copyright 2017 Elsevier. Schematic illustration of the SCC propagation and
523 lithium penetration into LLZO is shown in (b) and (d).
524

525 **Figure 2:** (a) Simulated average Li RMSD vs. simulation time with varying lattice parameters.
526 (b) Li self-diffusivity as a function of stress (positive stress means tension). The dotted lines
527 fitting the diffusivity with positive and negative slopes intersect at 2 GPa and a peak stress of 2.6
528 $\times 10^{-9}$ m²/s.
529

530 **Figure 3:** Schematic of using ion implantation to alter structure of solid electrolytes.

531